Dynamical generation of dark solitons in spin-orbit-coupled Bose-Einstein condensates

Shuai Cao,[1,2] Chuan-Jia Shan,[2,3] Dan-Wei Zhang,[2,4,*] Xizhou Qin,[5] and Jun Xu[5]

[1] *College of Sciences, South China Agricultural University, Guangzhou, 510642, China*

[2] *Laboratory of Quantum Engineering and Quantum Materials, and School of Physics and Telecommunication Engineering, South China Normal University, Guangzhou 510006, China*

[3] *College of Physics and Electronic Science, Hubei Normal University, Huangshi 435002, China*

[4] *Department of Physics and Center of Theoretical and Computational Physics, The University of Hong Kong, Pokfulam Road, Hong Kong, China*

[5] *State Key Laboratory of Optoelectronic Materials and Technologies, School of Physics and Engineering, Sun Yat-Sen University, Guangzhou 510275, China*

compiled: January 7, 2015

We numerically investigate the ground state, the Raman-driving dynamics and the nonlinear excitations of a realized spin-orbit-coupled Bose-Einstein condensate in a one-dimensional harmonic trap. Depending on the Raman coupling and the interatomic interactions, three ground-state phases are identified: stripe, plane wave and zero-momentum phases. A narrow parameter regime with coexistence of stripe and zero-momentum or plane wave phases in real space is found. Several sweep progresses across different phases by driving the Raman coupling linearly in time is simulated and the non-equilibrium dynamics of the system in these sweeps are studied. We find kinds of nonlinear excitations, with the particular dark solitons excited in the sweep from the stripe phase to the plane wave or zero-momentum phase within the trap. Moreover, the number and the stability of the dark solitons can be controlled in the driving, which provide a direct and easy way to generate dark solitons and study their dynamics and interaction properties.

OCIS codes: (020.0020) Atomic and molecular physics; (020.1475) Bose-Einstein condensates; (190.6135) Spatial solitons.

http://dx.doi.org/10.1364/XX.99.099999

1. Introduction

Spin-orbit (SO) coupling plays an important role in many fundamental quantum phenomena, ranging from the atomic fine structure to the newly discovered topological insulators [1, 2]. Recently, a synthetic SO coupling has been successfully engineered in Bose-Einstein condensations (BECs) and degenerate Fermi gases [3–12]. These cold atomic systems with adjustable SO coupling provide an ideal platform for investigating a wide range of interesting physics in many SO-coupled systems, such as atomic spin Hall effects [13, 14], Anderson localization of relativistic particles [15], fractional Fermi number [16] and topological superfluid with Majorana fermions [17]. The cold atoms with synthetic SO-coupling also have potential applications in designing atomic interferometry [18].

Since the newly realized SO-coupled BEC has no direct analog in solids, great attention has been paid to this unique many-body system. Especially, the ground state of SO-coupled BECs has been studied extensively in theory [19–38]. For a two-dimensional homogeneous bosonic gas with Rashba SO coupling, depending on the interatomic interactions, the ground state of the system exhibits two unconventional phases: a plane wave phase with condensate in a single momentum state and a stripe phase with condensate in two opposite momenta [19–21]. While for the realized SO-coupled BEC with equal contributions of Rashba and Dresselhaus SO couplings [3–9], it is found that the ground state belong to the two phases (the stripe phase and the plane wave phase) or the conventional zero-momentum phase, and thus an interesting tri-critical point was predicted in the phase diagram [22]. Taking the finite temperature [23], a harmonic trap [24–26] or a rotating trap [27–30] into account, more exotic phases were revealed, such as half vortices and Skyrmion lattices. Loading the SO-coupled bosons into optical lattices, many novel magnetic ground states were also found [36–38].

The dynamics of SO-coupled BECs has also been

* Corresponding author: zdanwei@126.com

studied in different contexts [5, 39–44]. For example, they have been demonstrated to exhibit unconventional collective dipole oscillations [5, 39] and spin dynamics [40, 41], interesting spin Josephson effects [42] and relativistic dynamics with analogs of Zitterbewegung [43] and Klein tunneling [44] under certain conditions. For the realized Rashba-Dresselhaus SO-coupled BEC, if the Raman coupling is driven in time, the system will pass through phase transition points. However, such Raman-driving dynamics in this system is yet to be explored.

On the other hand, the interatomic interactions in BECs lead to inherent nonlinearity under the Gross-Pitaevskii mean-field description. Thus the dynamics of a BEC is governed by a nonlinear Schrödinger equation, where the interaction strength could be tuned by Feshbach resonances [45]. With the tunable nonlinearity, the dark solitons [46, 47], bright solitons [48, 49], and gap solitons [50] in SO-coupled BECs are also investigated recently. Interestingly, the dark solitons can be excited by other methods. One can engineer a phase difference in a condensate to create a dark soliton at the interface between the phase domains [51] or merge two coherent condensates to create multiple dark solitons [52]. Other schemes of generating dark solitons involve driving the system away from equilibrium [53, 54], such as using nonlinearity-assisted quantum tunneling [55]. Thus, a natural question is whether we can dynamically generate the solitons in the realized SO-coupled BEC by the Raman-driving.

In this paper, we numerically investigate the Raman-driving dynamics and the nonlinear excitations of the realized SO-coupled BEC in a one-dimensional (1D) harmonic trap. By using imaginary time evolution method, we first obtain the ground state of the system and identify the three quantum phases depending on the Raman coupling strength and the interatomic interactions. Within the external trapping potential, we find a narrow parameter regime with coexistence of stripe and zero-momentum or plane wave phases in real space, which is absent in the homogenous case [22]. With the operator-splitting procedure, we then simulate four different sweeps across the ground-state phases by driving the Raman coupling linearly in time. In these sweeps, we study the non-equilibrium dynamics of the system and obtain different nonlinear excitations. Interestingly, we find that dark solitons can be excited within the trap in the sweep from the stripe phase to the plane wave or zero-momentum phase. Moreover, we show that the number and the stability of the dark solitons can be controlled in the dynamical progress, providing a direct and easy way to create dark solitons and study their dynamics and interaction properties.

The remaining part of this paper is organized as follows. We introduce the model for a SO-coupled BEC in a harmonic trap in Sec. II. The ground-state properties of the system are numerically studied in Sec. III. Then we investigate the Raman-driving dynamics and excitations in the sweeps across different ground-state phases in Sec. IV. Finally, a short summary is given in Sec. V.

2. The model

We consider a SO-coupled BEC confined in a quasi-1D harmonic trap with equal strength of Rashba and Dresselhaus SO couplings, which has been realized with ^{87}Rb atoms [3–9]. In the mean-field approach, the energy functional of the system is $E = \int_{-\infty}^{+\infty} \mathcal{E} dx$, with the energy density

$$\mathcal{E} = \frac{1}{2}\left(\Psi^\dagger \mathcal{H}_0 \Psi + g_{\uparrow\uparrow}|\psi_\uparrow|^4 + g_{\downarrow\downarrow}|\psi_\downarrow|^4 + 2g_{\uparrow\downarrow}|\psi_\uparrow|^2|\psi_\downarrow|^2\right), \tag{1}$$

where $\Psi \equiv (\psi_\uparrow, \psi_\downarrow)^T$ with $\psi_\uparrow$ and $\psi_\downarrow$ being the two (pseudo-) spin wave functions of the BEC, and the effective 1D interaction constants $g_{\sigma\sigma'} = 2\hbar^2 a_{\sigma\sigma'} N/(m l_\perp^2)$ are defined by the s-wave scattering lengths $a_{\sigma\sigma'}$ with $\sigma, \sigma' = \uparrow, \downarrow$, the particle number N and the oscillator length associated with a harmonic vertical confinement $l_\perp$. Hereafter we assume $g_{\uparrow\uparrow} = g_{\downarrow\downarrow} \equiv g_0$ and $g_{\uparrow\downarrow} = g_{\downarrow\uparrow} \equiv g_1$ for simplicity. The single particle Hamiltonian $\mathcal{H}_0$ in Eq. (1) is given by [3]

$$\mathcal{H}_0 = \frac{1}{2m}\left[(\hat{p}_x - k_0\sigma_z)^2\right] + \frac{\Omega}{2}\sigma_x + \frac{\delta}{2}\sigma_z + V_{\rm ext}, \tag{2}$$

where $m \simeq 1.44 \times 10^{-25}$ kg is ^{87}Rb atomic mass, $\hat{p}_x = -i\hbar\partial_x$ is the momentum operator, k_0 is the wave number of the Raman lasers for coupling the two hyperfine states, $\sigma_{x,z}$ are Pauli matrices, Ω is the Raman coupling strength, δ is an effective Zeeman field for the spin states, and $V_{\rm ext} = m\omega_x^2 x^2/2$ is the external trapping potential with frequency ω_x. We assume the typical trapping frequency $\omega_x = 2\pi \times 20$ Hz, such that $a_x = 2.4$ μm. We further assume $l_\perp = 0.1a_x$, $k_0 = 5a_x^{-1}$, and the total number of atoms $N \approx 10^5$. Then the interaction strengths g_0 and g_1 are on the range from several tens to several hundreds of $\hbar\omega_x$ for typical scattering lengths.

Measuring the length in units of $a_x = \sqrt{\hbar/(m\omega_x)}$, time in units of ω_x^{-1}, energy in units of $\hbar\omega_x$, we derive the dimensionless equations of motion for wave functions $\psi_{\uparrow,\downarrow}$ [47]:

$$\begin{aligned} i\partial_t\psi_\uparrow = &\frac{1}{2}(-i\partial_x - k_0)^2\psi_\uparrow + \frac{\delta}{2}\psi_\uparrow + V_{\rm ext}\psi_\uparrow + \\ &(g_0|\psi_\uparrow|^2 + g_1|\psi_\downarrow|^2)\psi_\uparrow + \frac{\Omega}{2}\psi_\downarrow, \end{aligned} \tag{3}$$

$$\begin{aligned} i\partial_t\psi_\downarrow = &\frac{1}{2}(-i\partial_x + k_0)^2\psi_\downarrow - \frac{\delta}{2}\psi_\downarrow + V_{\rm ext}\psi_\downarrow + \\ &(g_0|\psi_\downarrow|^2 + g_1|\psi_\uparrow|^2)\psi_\downarrow + \frac{\Omega}{2}\psi_\uparrow. \end{aligned} \tag{4}$$

Here we have used $\omega_x \to \omega_x/\omega_x = 1$, $k_0 \to a_x k_0$, $\delta \to \delta/(\hbar\omega_x)$ and $\Omega \to \Omega/(\hbar\omega_x)$, thus now $V_{\rm ext} = \frac{1}{2}x^2$.

In the following, we numerically minimize the energy functional to obtain the ground-state wave functions of the system described by Eq. (1) and Eqs. (3,4) for varying Raman coupling strength using the imaginary time evolution method. Then in the next section, we simulate the Raman-driving dynamics across different ground-state phases by integrating the equations of motion with

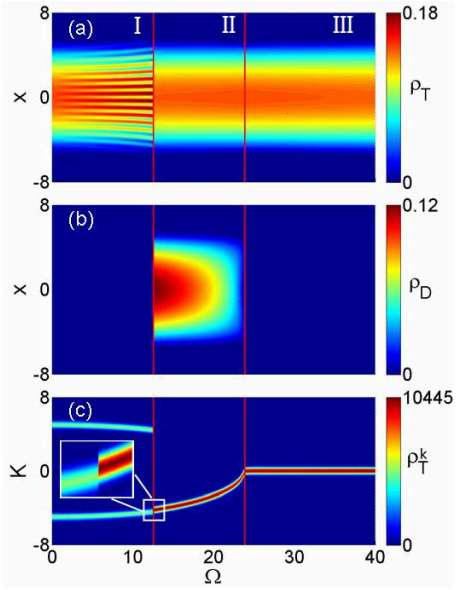

Fig. 1. (Color online) The ground states of the SO-coupled BEC for different Raman coupling strength Ω with the dimensionless parameters: $k_0 = 5$, $g_0 = 100$ and $g_1 = 80$. (a) The total density distribution of the ground state $\rho_T(x)$ in real space. (b) The difference density distribution of the two spin components $\rho_D(x)$ in real space. (c) The momentum distribution of the total density for the case in (a). The horizontal red lines correspond to the boundaries between different phases. Phases I, II, and III respectively denote the stripe phase, the plane wave phase, and the zero-momentum phase. The characteristics of the ground states in the three phases are in the text.

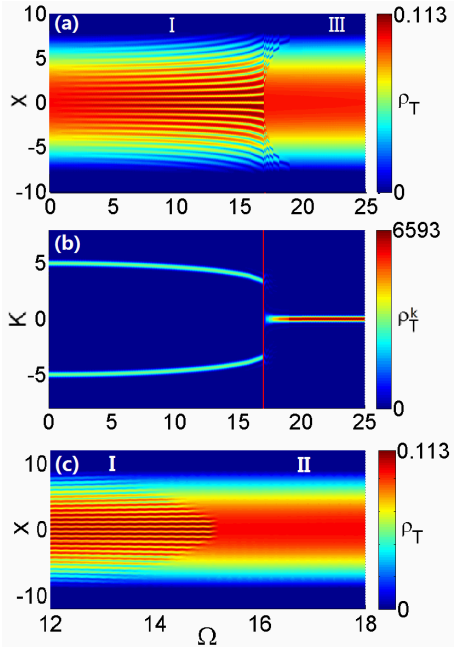

Fig. 2. (Color online) The ground states of the SO-coupled BEC for different Raman coupling strength Ω with the dimensionless interaction parameters: (a,b) $g_0 = 500$ and $g_1 = 100$; (c) $g_0 = 500$ and $g_1 = 400$. (a,c) The total density distribution of the ground state $\rho_T(x)$. (b) The corresponding momentum distribution of the total density. The horizontal red lines correspond to the boundary between phases I and III. The coexistence of phases I and III in a small region near the critical Raman coupling strength is characterized by Gaussian density distribution in the trap center with stripe density at the edge as shown in (a), and the coexistence of phases I and II is characterized by Gaussian density distribution at the edge with stripe density in the center as shown in (c). Other parameters in (a-c) is $k_0 = 5$.

the well-developed operator-splitting procedure. In the following numerical calculations, we will mainly consider $\delta = 0$ for simplicity.

In simulations, we fix $k_0 = 5$ and mainly consider two typical groups of interaction parameters: $g_0 = 100$ and $g_1 = 80$ as the first case, $g_0 = 500$ and $g_1 = 100$ as the second case. The reason for our choice is that they respectively give rise to the three and two ground-state phases and meanwhile within the typical experimental parameter range. However, we note that the ground-state properties and the Raman-driving dynamics with excited dark solitons, which will be discussed in the following two sections, mostly remain for different choices of interaction parameters. In experiments, the values of g_0 and g_1 may be directly changed by varying the transverse trapping strength, but the ratio g_0/g_1 is fixed in this way.

3. Ground states

The system in the uniform case ($V_{\rm ext} = 0$) has been well studied in Ref. [22], and it is analytically found that if the SO-coupling dominates and the condition $k_0^2 > G_- + \frac{G_-}{4G_+}$ is satisfied with $G_\pm \equiv g_0 \pm g_1$, there are three different phases with interesting condensate states for varying Raman coupling strength [22]. However, if the atomic interactions dominate and the condition is not satisfied, there are two condensate states [22]. Even though the boundary condition can not be solved analytically in the presence of a trapping potential, our simulations demonstrate that the two cases also appear. The numerical results of the ground states are shown in Fig. 1 and Fig. 2, corresponding to the two groups of interaction parameters, respectively. Here we plot the total density for the ground state wave functions ρ_T and the difference density between two spin components ρ_D (spin polarization) in real space as a function of Raman coupling strength, with

$$\rho_T \equiv |\psi_\uparrow(x)|^2 + |\psi_\downarrow(x)|^2,$$
$$\rho_D \equiv |\psi_\uparrow(x)|^2 - |\psi_\downarrow(x)|^2. \quad (5)$$

We also plot the total density in the momentum space $\rho_T^k \equiv |\psi_\uparrow(k)|^2 + |\psi_\downarrow(k)|^2$, where the wave function $\psi_\sigma(k) = \frac{1}{\sqrt{2\pi}} \int_{-\infty}^{+\infty} \psi_\sigma(x) e^{ikx} dx$. We will see that ρ_T, ρ_D and ρ_T^k together characterize different condensate states, with the central momentum of the condensate and the

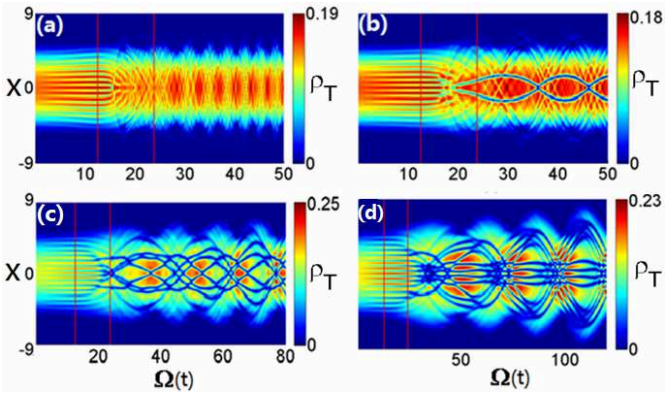

Fig. 3. (Color online) The density evolution $\rho_T(x,t)$ in the sweep from phase I to phase II by Raman driving $\Omega(t) = \Omega_0 + \beta t$ with $\Omega_0 = 0.5$ and typical sweep rates β: (a) $\beta = 0.6$, (b) $\beta = 1.5$, (c) $\beta = 3$ and (d) $\beta = 6$. The horizontal red lines corresponds to the phase transition points. Other parameters are $k_0 = 5$, $g_0 = 100$ and $g_1 = 80$.

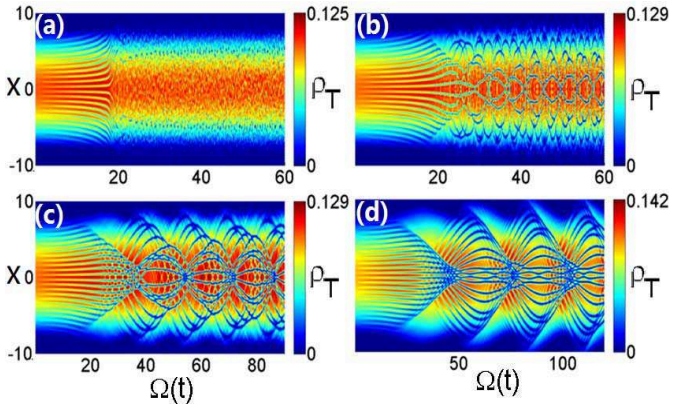

Fig. 4. (Color online) The density evolution $\rho_T(x,t)$ in the sweep from phase I to phase III by Raman driving $\Omega(t) = \Omega_0 + \beta t$ with $\Omega_0 = 0.5$ and typical sweep rates β: (a) $\beta = 0.1$, (b) $\beta = 0.6$, (c) $\beta = 3$ and (d) $\beta = 6$. Other parameters are $k_0 = 5$, $g_0 = 500$, and $g_1 = 100$.

spin polarization being the order parameters [22].

We first consider the case that the SO-coupling dominates with $k_0 = 5$, $g_0 = 100$ and $g_1 = 80$. As shown in Fig. 1, three ground-state phases are respectively denoted by phases I, II and III with increasing Ω, and their boundaries are marked by the red solid lines. Phase I is the stripe phase for relatively small Ω, characterized by fringes in the density ρ_T in Fig. 1(a). In this phase, the atoms condense in an equal-probability superposition of two plane waves with opposite wave vectors as shown in Fig. 1(c). Besides, the spin polarization identically vanishes, leading to $\rho_D = 0$ in Fig. 1(b). It is interesting to note that if $\delta \neq 0$, the spin symmetry will be broken and then the phase separation of the ground-state BEC can appear in the regime of phase I, which has been observed in experiments [3, 5]. We have numerically confirmed the appearance of phase separation for finite δ and above a critical Raman coupling strength in the regime of Phase I, which is not shown in Fig. 1 for the $\delta = 0$ case.

Phase II is the plane wave phase for intermediate Ω, characterized by a single non-zero momentum peak in ρ_T^k and finite spin polarization. Phase III is the zero-momentum phase for relatively large Ω, where the central momentum of the condensate is zero and the spin polarization also vanishes. The phase transition between I and II belongs to the first order phase transition with a jump in the central momentum as shown in the insert figure in Fig. 1(c). While the one between II and III belongs to the second order phase transition. In all of the three phases, the overall density configuration exhibits a Gaussian distribution due to the external harmonic trap, which also demonstrates that the local density approximation works well here.

For the case that the interactions dominate with $k_0 = 5$, $g_0 = 500$ and $g_1 = 100$, the results of the ground states are shown in Fig. 2. In this case, we can see that there are only phases I and III. The phase transition between I and III belongs to the first order phase transition. Interestingly, we find the coexistence of the two phases in a small region near the critical Raman coupling strength, characterized by Gaussian density distribution in the trap center with stripe density in the edge as shown in Fig. 2(a). This phenomenon is due to the inhomogeneous interaction effect by the trapping potential, which is absent in the homogenous case [22]. In the local density approximation, the density distribution of atoms is inhomogeneous and decrease away from the center of the trap, leading to the decreasing interaction strength from the center to the edge. Since the interactions play an crucial role in this case and the critical Raman coupling strength between phases I and III depends on the interaction strength, the central part of the condensate will enter into the phase III earlier than the edge when increasing Raman coupling.

One may also expect a coexistence of stripe and plane wave phases in real space from the same mechanism, which is absent for the case in Fig. 1 due to the weak interactions. Actually, for appropriately intermediate interaction strengths, the I-II coexistence phase is indeed found in our numerical simulations. An example is shown in Fig. 2(c) for $g_0 = 500$ and $g_1 = 400$, where the I-II coexistence phase is characterized by Gaussian density distribution at the edge with stripe density in the center. This result further demonstrates that the two coexistence phases are not always present in the whole interaction parameter regime and actually from the competitions between repulsive interactions and external trapping.

4. Raman-driven dynamics and generation of dark solitons

In this section, we consider the quantum dynamics and excitations of the SO-coupled BEC in the sweeps be-

tween three ground-state phases. To do this, the system is initially prepared in one of its ground states, and is then driven across the phase transition points by the Raman-driving, which can be achieved by changing the intensity of the Raman lasers in experiments. We consider that the Raman coupling strength varies linearly in time t:

$$\Omega(t) = \Omega_0 + \beta t, \tag{6}$$

where Ω_0 is the Raman coupling strength at $t = 0$ and β is the Raman-driving rate. The ground states depend on Ω_0, g_0 and g_1, with the phase boundaries shown in Figs. 1 and 2. In the following, we numerically simulate these sweeping progresses by integrating the equations of motion (3) and (4).

4.A. Dark solitons in I-II and I-III sweeps

We first consider the sweep from phase I to phase II with typical interaction strengths $g_0 = 100$ and $g_1 = 80$. At the outset the Raman coupling $\Omega_0 = 0.5$, and the atoms condense into the stripe ground state within the region of phase I, which is obtained numerically by the imaginary time evolution method. Then the Raman coupling strength is increased as the form given by Eq. (6). The numerical results of the Raman-driving dynamics for some typical sweeping rates β are shown in Fig. 3, where we plot the density evolution of the SO-coupled BEC $\rho_T(x, t)$. Here the two horizontal red lines denote the phase boundaries. For slow sweep with $\beta = 0.6$ as shown in Fig. 3(a), the BEC begins to oscillate after passing through the first phase transition point between I and II and then gradually exhibits breathing oscillation. The amplitude and frequency of the breathing oscillation characterize the propagation of excitation modes, which are different from the sound modes in this system when subjected to a perturbation driving [22]. We have also checked that in the very slow sweeping limit, the system will evolve adiabatically without collective excitations (which is not shown here).

When the sweep is fast enough with $\beta = 1.5$, we find that a pair of dark solitons exhibit in the BEC after passing through the phase transition point as shown in Fig. 3(b). The dark solitons are generated in the center because the nonlinear interactions are stronger there within the external harmonic trap. Due to the harmonic force, the solitons are reflected from the edges of the trap and collide in the center again and again, giving rise to the oscillation behavior of the dark solitons and interference pattern in Fig. 3(b). When increasing the sweep rate with $\beta = 3, 6$ as shown in Figs. 3(c,d), more and more dark soltions are excited in the system with similar oscillation dynamics and interference pattern.

We then consider the sweep from phase I to phase III with typical interaction strengths $g_0 = 500$ and $g_1 = 100$, which is also the first order phase transition. We also set the system initially in the ground state with $\Omega_0 = 0.5$ and the Raman coupling is increased linearly in time. The numerical results of the evolution of atomic density $\rho_T(x, t)$ are shown in Fig. 4 for different sweep rates. For very slow sweep with $\beta = 0.1$ as shown in Fig. 4(a), neither dark solitons nor breathing modes are excited in the BEC in this case. While for $\beta = 0.6$ in Fig. 4(b), we find that more than one pair of dark solitons are generated compared to the I-II sweep with the same sweeping rate in Fig. 3(a). This is due to the facts that the stronger atomic interaction in this case leads to more density dips for the dynamical generation of dark solitons. In this case, also more and more dark solitons are excited with similar oscillation and interference dynamics when increasing the sweep rate with $\beta = 3, 6$ as shown in Figs. 4(c,d). In a word, the dark solitons are more easily excited in the I-III sweep than in the I-II sweep.

We should note that the boundaries among the three ground-state phases and the corresponding spin polarization will be modified for the case $\delta \neq 0$, which corresponds to broken spin symmetry [22]. However, we have numerically confirmed that the dark solitons can also be created in these non-adiabatic sweeps for $\delta \neq 0$. Moreover, this way of generation of dark solitons is not specific to the particular choices of interaction and SO-coupling strengths as those in Figs. 3 and 4. As long as the sweeps are from the stripe ground state and fast enough, the dark solitons will be excited and exhibit oscillatory motion and collision in the trap. In contract, the existence of solitons in SO-coupled BECs in previous work closely relies on certain particular conditions, such as ring-shape trapping potentials [46], stationary points in the dispersion relation [47], attractive interactions [48, 49] and spatially periodic Zeeman fields [50]. Therefore, our work demonstrated a general method of dynamically generating solitons in SO-coupled BECs, which is easy to be implemented in current experiments without carefully designing the Raman lasers and atomic interactions.

4.B. Formation, stability and dynamics of the excited dark solitons

In this part, we further discuss the formation, stability and dynamics of the excited dark solitons in the sweeps. In experiments, one could use the phase imprinting and density engineering methods to create dark solitons in an ordinary BEC [51, 52]. However, the different mechanism of dynamically generating dark solitons here is by sweeping the BECs away from equilibrium stripe ground states and across phase boundaries [53, 54]. In a harmonically trapped condensate with repulsive interatomic interactions, the nodes of the excited nonlinear eigenstates can evolve into the dark solitons [55, 56].

For the stripe condensate, there are many dips in its density distribution to support the formation of dark solitons when the system is driven fast enough from phase I to phase II, as shown in Figs. 3(b-d). To see this point more clearly, we first plot the spin-up-component density $|\psi_\uparrow(x)|^2$ and the phase $\varphi_\uparrow(x)$ of the stripe ground state in Fig. 5(a). Even though the phase is rela-

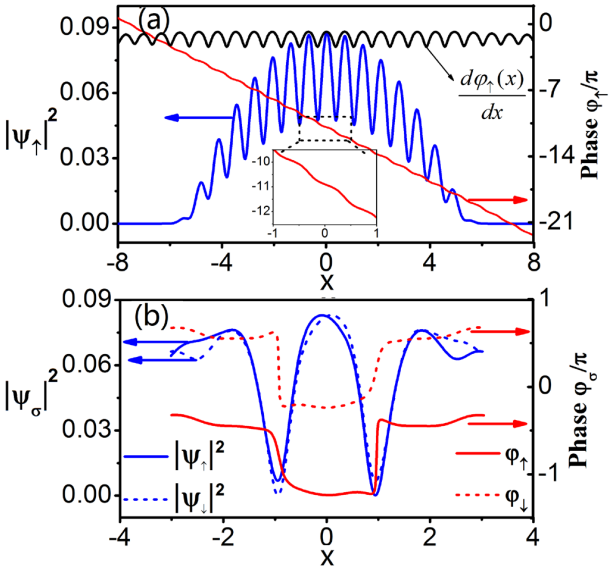

Fig. 5. (Color online) (a) The spin-up-component density $|\psi_\uparrow(x)|^2$ (blue solid) and phase $\varphi_\uparrow(x)$ (red solid) of the stripe ground state for $\Omega = 12$. The black solid line denotes the spatial derivative of the phase $d\varphi_\uparrow(x)/dx$, which shows maximum phase variation at the density dips. (b) The density $|\psi_\sigma(x)|^2$ (blue solid line for $\sigma =\uparrow$ and blue dashed line for $\sigma =\downarrow$) and phase $\varphi_\sigma(x)$ (red solid line for $\sigma =\uparrow$ and red dashed line for $\sigma =\downarrow$) of the excited dark solitons when $\Omega(t) = 50$ in Fig. 3(b). Other parameters are $k_0 = 5$, $g_0 = 100$, $g_1 = 80$ and $\beta = 1.5$.

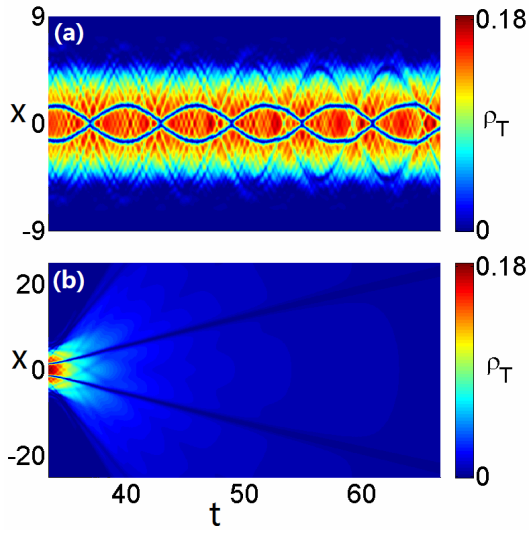

Fig. 6. (Color online) The stability of the dark solitions in Fig. 3(b). The long-time evolution of the total density $\rho_T(x,t)$ for: (a) keeping on the trapping potential; and (b) turning off the trapping potential, after stopping the Raman driving at time $t_d = 33$. Other parameters are $k_0 = 5$, $g_0 = 100$, $g_1 = 80$, $\Omega_0 = 0.5$ and $\beta = 1.5$.

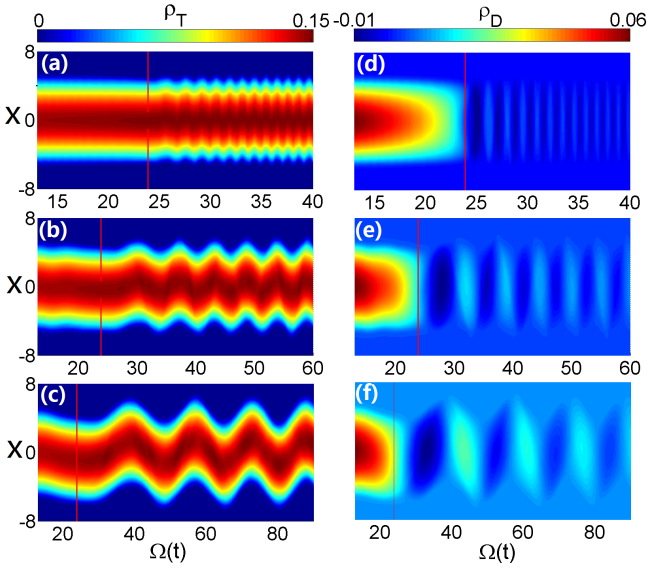

Fig. 7. (Color online) The density evolutions $\rho_T(x,t)$ and $\rho_D(x,t)$ in the sweep from phase II to phase III by Raman driving $\Omega(t) = \Omega_0 + \beta t$ with $\Omega_0 = 13$ and typical sweep rates β: (a) and (d) $\beta = 0.1$, (b) and (e) $\beta = 0.6$, (c) and (f) $\beta = 2$. The horizontal red lines correspond to the phase transition point. Other parameters are $k_0 = 5$, $g_0 = 100$ and $g_1 = 80$.

tively smooth in space, the maximum phase variation $d\varphi_\uparrow(x)/dx$ locates at the density dips, which is favorable to form dark solitons. The situations of the spin-down component are similar. We then plot the spin density $|\psi_\sigma(x)|^2$ and the phase $\varphi_\sigma(x)$ of the excited dark solitons [when $\Omega(t) = 50$ in Fig. 3(b)] in Fig. 5(b), where the density dips and the accompanied phase jumps of the two dark solitons can be seen clearly.

To verify the stability of the generated dark solitons in Fig. 6, we calculate the long-time evolution of atomic density $\rho_T(x,t)$ after the driving time $t_d = 33$, corresponding to $\Omega(t_d) = 50$ and the same parameters in Fig. 3(b). Figures 6(a) and 6(b) correspond to the cases of keeping on and tuning off the trap when the driving is stopped at $t = t_d$, respectively. It is clear from Fig. 6(a) that the dark solitons remain periodically oscillating in the trap after stopping driving, without significant decay for a long time. Therefore we can conclude that the dark solitons in this system are stable within the trapping potential. If the trap is also turned off with the driving, the dark solitons will propagate and spread out, which is shown in Fig. 6(b).

For an equilibrium SO-coupled BEC without driving, the analytical single-dark-soliton solution of Eqs. (3,4) can be approximately obtained as the forms in Ref. [47]. However, for the non-equilibrium system with multiple interacting dark solitons here, it is too complicated to get the analytical forms and derive an effective model to exactly describe their dynamics as shown in Figs. 3 and Fig. 4. In Ref. [47], the size of a single dark soliton is characterized to be proportional to an effective healing length, which is determined by the atomic interaction strengths and the stationary points in the dispersion relation. In numerical simulations for our case, we

can not find a clear and direct connection between the size of excited multiple dark solitons and the (effective) healing length. For the simplest two-soliton case in Figs. 3(b) and 6(a), the dark solitons clearly show particle-like behaviors with oscillatory motion and mutually interactions within the external trap, which has been observed in ordinary BECs [52]. For well-separated dark solitons, their center $X_0(t)$ approximately satisfies the equation of motion in the form $d^2X_0/dt^2 = -\frac{1}{2}M_0\omega_s^2X_0$, where M_0 is the effective mass of the dark solitons [47] and ω_s is the oscillation frequency determined by the harmonic trap [51, 52]. Due to the interactions between dark solitons, which can be treated by additional potentials, the oscillation frequencies of interacting are modified [52]. In addition, as the non-adiabatic driving does, the motion and collision of multiple dark solitons gradually generate excitation modes in the SO-coupled BEC, resulting in the complicated breathing-like behavior in the background as shown in Figs. 3(c,d) and 4(c,d). Clearly, the oscillation amplitude of the multiple dark solitons does not remain constant in this case.

4.C. Dynamics in sweeps between phases II and III

Now we turn to consider the sweeps between phase II and phase III. The first case we considered is the sweep from phases II to III, which belongs to the second order phase transition. To do this, we set the system initially in phase II with $\Omega_0 = 13$ and choose the same interaction parameters as those in Fig. 3: $g_0 = 100$ and $g_1 = 80$. Then the Raman coupling is also increased linearly in time. In this case, the collective center-of-mass (COM) motion in $\rho_T(x,t)$ and the periodical oscillation of the spin polarization in $\rho_D(x,t)$ can emerge, with two examples being shown in Figs. 7(a,d) and 7(b,e) for $\beta = 0.1$ and $\beta = 0.6$, respectively. It is clear to see from Fig. 7 that for very slow sweep ($\beta = 0.1$), the system almost follows its ground state in the beginning and then exhibits the dynamical oscillation once passing through the phase transition point. In addition, the period and the amplitude of the oscillation are both increased by increasing the Raman driving rate. However, we find that the dark solitons can not be excited by the Raman-driving even in the fast sweep, such as $\beta = 2$ in Figs. 7(c,f), which just exhibit similar oscillating COM motion and spin dynamics. We have also checked that no dark soliton can be excited in a much faster sweep in this case. This is due to the absence of density dips in the initial plane-wave state to evolve into dark-soliton excitations. Since the dark solitons can be excited only from the stripe state, the appearance of dark solitons in the Raman driving is an indication of the existence of stripe state, which has not directly been imaged in experiments [3, 5].

To further study the COM motion of the system, we calculate the corresponding population evolution of the two spin components as $P_\sigma(t) = \int_{-\infty}^{+\infty} |\psi_\sigma(x,t)|^2 dx$ and

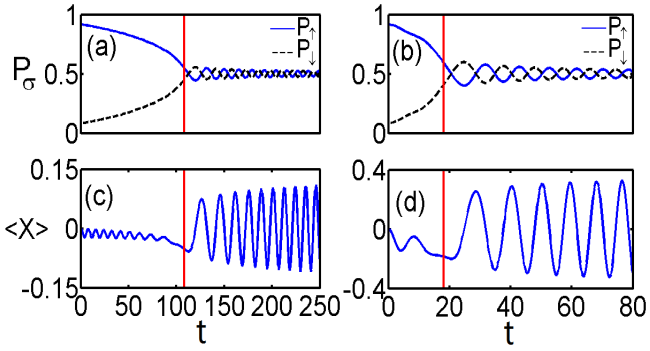

Fig. 8. (Color online) The population evolution of the spin components $P_\sigma(t)$ in (a) and (b), and the center-of-mass evolution in (c) and (d) for the II-III sweep. The horizontal red line corresponds to the phase transition point. The driving rates are $\beta = 0.1$ in (a) and (c), and $\beta = 0.6$ (b) and (d). Other parameters in (a-d) are $\Omega_0 = 13$, $k_0 = 5$, $g_0 = 100$ and $g_1 = 80$.

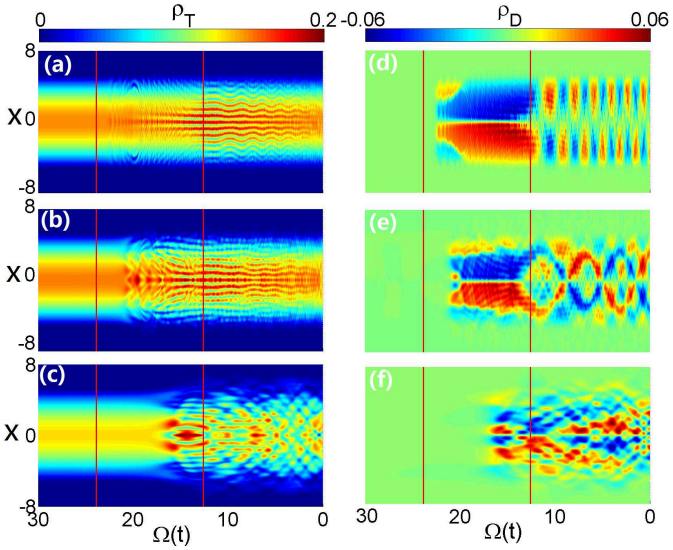

Fig. 9. (Color online) The density evolutions $\rho_T(x,t)$ and $\rho_D(x,t)$ in the inverse sweep from phase III to phase II by Raman driving $\Omega(t) = \Omega_0 + \beta t$ with $\Omega_0 = 30$ and typical sweep rates β: (a) and (d) $\beta = -0.1$, (b) and (e) $\beta = -0.4$, (c) and (f) $\beta = -2$. The horizontal red lines corresponds to the phase transition points. Other parameters are $k_0 = 5$, $g_0 = 100$ and $g_1 = 80$.

the COM evolution as

$$\langle x(t)\rangle = \int_{-\infty}^{+\infty} \left[|\psi_\uparrow(x,t)|^2 + |\psi_\downarrow(x,t)|^2\right] x dx. \quad (7)$$

As shown in Fig. 8(a,b), the atoms initially condense mainly in one of two spins components, then their populations tend to be equal by the Raman driving and finally exhibit periodical oscillation after passing through the II-III phase transition point. However, both of the period and the amplitude of the spin-population oscillation decrease in time. As for the COM motion shown in

Fig. 8(c,d), the oscillation appears in the beginning even with very slow sweep [such as $\beta = 0.1$ in Fig. 8(c)], but its amplitude is very small because the system almost follows its ground state. We note that the oscillation in this case is similar to the well-known Zitterbewegung, which has been observed in the SO-coupled BECs [6, 7]. After passing through the transition point, the oscillating COM motion recovers and the oscillation amplitude is greatly enlarged and can be further increased by increasing the Raman-driving rate.

At the end of this part, we consider the inverse sweep, i.e., the sweep from phase III to phase II. The calculated density evolutions $\rho_{T,D}(x,t)$ are shown in Fig. 9, where the initial state of the system is in the phase III regime with $\Omega_0 = 30$ and the Raman coupling is decreased linearly in time with the rates $\beta = -0.1$ [Figs. 9(a,d)], $\beta = -0.4$ [Figs. 9(b,e)] and $\beta = -2$ [Figs. 9(c,f)]. In these cases, the system can follow its ground state with zero spin polarization at the beginning. As shown in Fig. 9, the longitudinal spin polarization of the system becomes finite and finally the excitations appear in the spin density with periodic oscillation after the system passes through the III-II phase boundary, and the excitations increase and the spin oscillation becomes more complicated when speeding up the driving. In this sweep, there is also no excited dark soliton for the same reason.

5. Conclusions

In conclusion, we have numerically studied the ground states of a 1D SO-coupled BEC in a harmonic trap and the Raman-driving dynamics across different ground-state phases. We found the coexistence of stripe and zero-momentum or plane wave phases in real space due to the the competitions between repulsive interactions and external trapping. We also showed a new method of dynamical generation of dark solitons in the Raman-driving by sweeping the BEC through the phase transition points. Both of the number and the stability of the excited dark solitons can be controlled in this direct and convenient way. Therefore, this system may provide a controllable platform for creating dark solitons and studying their dynamics and interaction properties. In view of the fact that the investigated SO-coupled BEC with adjustable Raman coupling strength has been realized by several experimental groups [3–9], it is anticipated that our predictions in this work can be tested in an experiment in the near future.

Acknowledgments

We thank Profs. Shi-Liang Zhu, Chaohong Lee and Biao Wu for many helpful discussions. This work was supported by the NSF (Grant No. 11404108), the PCSIRT and the SRFGS of SCNU. D. W. Z. acknowledges support from the postdoctoral fellowship of HKU.

References

[1] M. Z. Hasan and C. L. Kane, "Colloquium: Topological insulators," Rev. Mod. Phys. **82**, 3045 (2010).

[2] X.-L. Qi and S.-C. Zhang, "Topological insulators and superconductors," Rev. Mod. Phys. **83**, 1057 (2011).

[3] Y.-J. Lin, K. Jiménez-García, and I. B. Spielman, "Spin-orbit-coupled Bose-Einstein condensates," Nature (London) **471**, 83 (2011).

[4] R. A. Williams, L. J. LeBlanc, K. Jiménez-García, M. C. Beeler, A. R. Perry, W. D. Phillips, and I. B. Spielman, "Synthetic partial waves in ultracold atomic collisions," Science **335**, 314 (2011).

[5] J.-Y. Zhang, S.-C. Ji, Z. Chen, L. Zhang, Z.-D. Du, B. Yan, G.-S. Pan, B. Zhao, Y.-J. Deng, H. Zhai, S. Chen, and J.-W. Pan, "Collective dipole oscillations of a spin-orbit coupled Bose-Einstein condensate," Phys. Rev. Lett. **109**, 115301(2012).

[6] C. Qu, C. Hamner, M. Gong, C. Zhang, and P. Engels, "Observation of Zitterbewegung in a spin-orbit-coupled Bose-Einstein condensate," Phys. Rev. A **88**, 021604 (2013).

[7] L. J. LeBlanc, M. C. Beeler, K. Jimenez-Garcia, A. R. Perry, S. Sugawa, R. A. Williams, and I. B. Spielman, "Direct observation of zitterbewegung in a Bose-Einstein condensate," New J. Phys. **15**, 073011 (2013).

[8] A. J. Olson, S.-J. Wang, R. J. Niffenegger, C.-H. Li, C. H. Greene, and Y. P. Chen, "Tunable Landau-Zener transitions in a spin-orbit-coupled Bose-Einstein condensate," Phys. Rev. A **90**, 013616 (2014).

[9] J.-Y. Zhang, S.-C. Ji, L. Zhang, Z.-D. Du, W. Zheng, Y.-J. Deng, H. Zhai, S. Chen, and J.-W. Pan, "Experimental determination of the finite-temperature phase diagram of a spin-orbit coupled Bose gas," Nat. Phys. **10**, 314 (2014).

[10] P. Wang, Z. Q. Yu, Z. Fu, J. Miao, L. Huang, S. Chai, H. Zhai, and J. Zhang, "Spin-orbit coupled degenerate Fermi gases," Phys. Rev. Lett. **109**, 095301 (2012).

[11] L. W. Cheuk, A. T Sommer, Z. Hadzibabic, T. Yefsah, W. S. Bakr, and M. W. Zwierlein, "Spin-injection spectroscopy of a spin-orbit coupled Fermi gas," Phys. Rev. Lett. **109**, 095302 (2012).

[12] Z. Fu, L. Huang, Z. Meng, P. Wang, L. Zhang, S. Zhang, H. Zhai, P. Zhang, and J. Zhang, "Production of Feshbach molecules induced by spin-orbit coupling in Fermi gases," Nat. Phys. **10**, 110 (2014).

[13] S.-L. Zhu, H. Fu, C.-J. Wu, S.-C. Zhang, and L.-M. Duan, "Spin Hall effects for cold atoms in a light-induced gauge potential," Phys. Rev. Lett. **97**, 240401 (2006); X.-J. Liu, X. Liu, L. C. Kwek, and C. H. Oh, "Optically induced spin-Hall effect in atoms," Phys. Rev. Lett. **98**, 026602 (2007).

[14] M. C. Beeler, R. A. Williams, K. Jiménez-García, L. J. LeBlanc, A. R. Perry, and I. B. Spielman, "The spin Hall effect in a quantum gas," Nature **498**, 201 (2013).

[15] S.-L. Zhu, D.-W. Zhang, and Z. D. Wang, "Delocalization of relativistic Dirac particles in disordered one-dimensional systems and its implementation with cold atoms," Phys. Rev. Lett. **102**, 210403 (2009); D.-W. Zhang, Z. D. Wang, and S.-L. Zhu, "Relativistic quantum effects of Dirac particles simulated by ultracold atoms," Front. Phys. **7**, 31 (2012).

[16] D.-W. Zhang, L.-B. Shao, Z.-Y. Xue, H. Yan, Z. D. Wang, and S.-L. Zhu, "Particle-number fractionalization of a one-dimensional atomic Fermi gas with synthetic spin-orbit coupling," Phys. Rev. A **86**, 063616 (2012).

[17] C. Zhang, S. Tewari, R. M. Lutchyn, and S. Das Sarma,"px+ipy superfluid from s-wave interactions of

fermionic cold atoms," Phys. Rev. Lett. **101**, 160401 (2008); M. Sato, Y. Takahashi, and S. Fujimoto, "Non-Abelian topological order in s-wave superfluids of ultracold fermionic atoms," Phys. Rev. Lett. **103**, 020401 (2009); S.-L. Zhu, L.-B. Shao, Z. D. Wang, and L.-M. Duan, "Probing non-Abelian statistics of Majorana fermions in ultracold atomic superfluid," Phys. Rev. Lett. **106**, 100404 (2011).

[18] B. M. Anderson, J. M. Taylor, and V. M. Galitski, "Interferometry with synthetic gauge fields," Phys. Rev. A **83**, 031602(R) (2011); Y.-X. Du, H. Yan, D.-W. Zhang, C.-J. Shan, and S.-L. Zhu, "Proposal for a rotation-sensing interferometer with spin-orbit-coupled atoms," Phys. Rev. A **85**, 043619 (2012).

[19] C. Wang, C. Gao, C.M. Jian, and H. Zhai, "Spin-orbit coupled spinor Bose-Einstein condensates," Phys. Rev. Lett. **105**, 160403 (2010).

[20] T.-L. Ho and S. Zhang, "Bose-Einstein condensates with spin-orbit interaction," Phys. Rev. Lett. **107**, 150403 (2011).

[21] C. Wu, I. M. Shem, and X.-F. Zhou, Unconventional Bose- Einstein condensations from spin-orbit coupling, Chin. Phys. Lett. 28, 097102 (2011); X. Zhou, Y. Li, Z. Cai, and C. Wu, Unconventional states of bosons with synthetic spin-orbit coupling, J. Phys. B 46, 134001 (2013).

[22] Y. Li, L. P. Pitaevskii, and S. Stringari, "Quantum tricriticality and phase transitions in spin-orbit coupled Bose-Einstein condensates," Phys. Rev. Lett. **108**, 225301 (2012); Y. Li, L. P. Pitaevskii, and S. Stringari, "Sum rules, dipole oscillation and spin polarizability of a spin-orbit coupled quantum gas," Euro. Phys. Lett. **99**, 56008 (2012); G. I. Martone, Y. Li, L. P. Pitaevskii, and S. Stringari, "Anisotropic dynamics of a spin-orbit-coupled Bose-Einstein condensate," Phys. Rev. A **86**, 063621 (2012).

[23] C. M. Jian and H. Zhai, "Paired superfluidity and fractionalized vortices in systems of spin-orbit coupled bosons," Phys. Rev. B **84**, 060508 (2011).

[24] H. Hu, B. Ramachandhran, H. Pu, and X. J. Liu, "Spin-orbit coupled weakly interacting Bose-Einstein condensates in harmonic traps," Phys. Rev. Lett. **108**, 010402 (2012).

[25] Z. F. Xu, Y. Kawaguchi, L. You, and M. Ueda, "Symmetry classification of spin-orbit-coupled spinor Bose-Einstein condensates," Phys. Rev. A **86**, 033628 (2012).

[26] T. Ozawa and G. Baym, "Striped states in weakly trapped ultracold Bose gases with Rashba spin-orbit coupling," Phys. Rev. A **85**, 063623 (2012).

[27] S. Sinha, R. Nath, and L. Santos, "Trapped two-dimensional condensates with synthetic spin-orbit coupling," Phys. Rev. Lett. **107**, 270401(2011).

[28] X. F. Zhou, J. Zhou, and C. Wu, "Vortex structures of rotating spin-orbit-coupled Bose-Einstein condensates," Phys. Rev. A **84**, 063624 (2011).

[29] J. Radic, T. A. Sedrakyan, I. B. Spielman, and V. Galitski, "Vortices in spin-orbit-coupled Bose-Einstein condensates," Phys. Rev. A **84**, 063604 (2011).

[30] X. Q. Xu and J. H. Han, "Spin-orbit coupled Bose-Einstein condensate under rotation," Phys. Rev. Lett. **107**, 200401 (2011).

[31] Z.-Q. Yu, "Ground-state phase diagram and critical temperature of two-component Bose gases with Rashba spin-orbit coupling," Phys. Rev. A **87**, 051606 (2013).

[32] B. Ramachandhran, Hui Hu, and Han Pu, "Emergence of topological and strongly correlated ground states in trapped Rashba spin-orbit-coupled Bose gases," Phys. Rev. A **87**, 033627 (2013).

[33] P.-S. He, W.-L. You, and W.-M. Liu, "Stability of a two-dimensional homogeneous spin-orbit-coupled boson system," Phys. Rev. A **87**, 063603 (2013).

[34] T. Ozawa and G. Baym, "Condensation transition of ultracold Bose gases with rashba spin-orbit coupling," Phys. Rev. Lett. **110**, 085304 (2013).

[35] Q. Zhou and X. Cui, "Fate of a Bose-Einstein condensate in the presence of spin-orbit coupling," Phys. Rev. Lett. **110**, 140407 (2013).

[36] T. Graβ, K. Saha, K. Sengupta, and M. Lewenstein, "Quantum phase transition of ultracold bosons in the presence of a non-Abelian synthetic gauge field," Phys. Rev. A **84**, 053632 (2011); W. S. Cole, S. Zhang, A. Paramekanti, and N. Trivedi, "Bose-Hubbard models with synthetic spin-orbit coupling: mott insulators, spin textures, and superfluidity," Phys. Rev. Lett. **109**, 085302 (2012); J. Radic, A. Di Ciolo, K. Sun, and V. Galitski, "Exotic quantum spin models in spin-orbit-coupled mott insulators," Phys. Rev. Lett. **109**, 085303 (2012); Z. Cai, X. Zhou, and C. Wu, "Magnetic phases of bosons with synthetic spin-orbit coupling in optical lattices," Phys. Rev. A **85**, 061605(R) (2012); S. Mandal, K. Saha, and K. Sengupta, "Superfluid-insulator transition of two-species bosons with spin-orbit coupling," Phys. Rev. B **86**, 155101 (2012).

[37] D.-W. Zhang, J.-P. Chen, C.-J. Shan, Z. D. Wang, and S.-L. Zhu, "Superfluid and magnetic states of an ultracold Bose gas with synthetic three-dimensional spin-orbit coupling in an optical lattice," Phys. Rev. A **88**, 013612 (2013).

[38] J. Zhao, S. Hu, J. Chang, P. Zhang, and X. Wang, "Ferromagnetism in a two-component Bose-Hubbard model with synthetic spin-orbit coupling," Phys. Rev. A **89**, 043611 (2014); Z. Xu, W. S. Cole, and S. Zhang, "Mott-superfluid transition for spin-orbit-coupled bosons in one-dimensional optical lattices," Phys. Rev. A **89**, 051604(R) (2014); M. Piraud, Z. Cai, I. P. McCulloch, and U. Schollwock, "Quantum magnetism of bosons with synthetic gauge fields in one-dimensional optical lattices: A density-matrix renormalization-group study," Phys. Rev. A **89**, 063618 (2014).

[39] E. van der Bijl and R. A. Duine, "Anomalous Hall conductivity from the dipole mode of spin-orbit-coupled cold-atom systems," Phys. Rev. Lett. **107**, 195302 (2011).

[40] I. V. Tokatly and E. Y. Sherman, "Spin dynamics of cold fermions with synthetic spin-orbit coupling," Phys. Rev. A **87**, 041602 (2013).

[41] S. S. Natu and S. Das Sarma, "Spin dynamics in a spin-orbit-coupled Fermi gas," Phys. Rev. A **88**, 033613 (2013).

[42] D.-W. Zhang, L.-B. Fu, Z. D. Wang, and S.-L. Zhu, "Josephson dynamics of a spin-orbit-coupled Bose-Einstein condensate in a double-well potential," Phys. Rev. A **85**, 043609 (2012); M. A. Garcia-March, G. Mazzarella, L. DellAnna, B. Juliá-Díaz, L. Salasnich, and A. Polls,"Josephson physics of spin-orbit-coupled elongated Bose-Einstein condensates," Phys. Rev. A **89**, 063607 (2014); R. Citro and A. Naddeo, "Spin-orbit coupled Bose-Einstein condensates in a double well,"

arXiv:1405.5356.

[43] Y. Zhang, L. Mao, and C. Zhang, "Mean-field dynamics of spin-orbit coupled Bose-Einstein condensates," Phys. Rev. Lett. **108**, 035302(2012); Y. Zhang, G. Chen, and C. Zhang, Sci. Rep. **3**, 1937(2013); S. Cao, D.-W. Zhang, H. Yan, and Z.-Y. Xue, "Observation of Zitterbewegung in a spin-orbit coupled atomic gas," JETP Lett. **98**, 858 (2014).

[44] D.-W. Zhang, Z.-Y. Xue, H. Yan, Z. D. Wang, and S.-L. Zhu, "Macroscopic Klein tunneling in spin-orbit-coupled Bose-Einstein condensates," Phys. Rev. A **85**, 013628 (2012).

[45] C. Chin, R. Girmm, P. Julienne, and E. Tiesinga, "Feshbach resonances in ultracold gases," Rev. Mod. Phys. **82**, 1225 (2010).

[46] O. Fialko, J. Brand, and U. Zülicke, "Soliton magnetization dynamics in spin-orbit-coupled Bose-Einstein condensates," Phys. Rev. A **85**, 051605(R) (2012).

[47] V. Achilleos, J. Stockhofe, P. G. Kevrekidis, D. J. Frantzeskakis, and P. Schmelcher, "Matter-wave dark solitons and their excitation spectra in spin-orbit coupled Bose-Einstein condensates," Euro. Phys. Lett. **103**, 20002 (2013).

[48] V. Achilleos, D. J. Frantzeskakis, P. G. Kevrekidis, and D. E. Pelinovsky, "Matter-wave bright solitons in spin-orbit coupled Bose-Einstein condensates," Phys. Rev. Lett. **110**, 264101 (2013).

[49] Y. Xu, Y. Zhang, and B. Wu, "Bright solitons in spin-orbit-coupled Bose-Einstein condensates," Phys. Rev. A **87**, 013614 (2013).

[50] Y. V. Kartashov, V. V. Konotop, and F. K. Abdullaev, "Gap solitons in a spin-orbit-coupled Bose-Einstein condensate," Phys. Rev. Lett. **111**, 060402 (2013); V. E. Lobanov, Y. V. Kartashov, and V. V. Konotop, "Fundamental, multipole, and half-vortex gap solitons in spin-orbit coupled Bose-Einstein condensates," Phys. Rev. Lett. **112**, 180403 (2014).

[51] S. Burger, K. Bongs, S. Dettmer, W. Ertmer, K. Sengstock, A. Sanpera, G. V. Shlyapnikov, M. Lewenstein, "Dark solitons in Bose-Einstein condensates," Phys. Rev. Lett. **83**, 5198 (1999); J. Denschlag, J. E. Simsarian, D. L. Feder, C. W. Clark, L. A. Collins, J. Cubizolles, L. Deng, E. W. Hagley, K. Helmerson, W. P. Reinhardt, S. L. Rolston, B. I. Schneider, W. D. Phillips, "Generating solitons by phase-engineering a Bose-Einstein condensate," Science **287**, 97 (2000); C. Becker, S. Stellmer, P. Soltan-Panahi, S. Dörscher, M. Baumert, E.-M. Richter, J. Kronjäger, K. Bongs, K. Sengstock, "Oscillations and interactions of dark and dark-bright solitons in Bose-Einstein condensates," Nat. Phys. **4**, 496 (2008).

[52] A. Weller, J. P. Ronzheimer, C. Gross, J. Esteve, M. K. Oberthaler, D. J. Frantzeskakis, G. Theocharis, and P. G. Kevrekidis, "Experimental observation of oscillating and interacting matter wave dark solitons," Phys. Rev. Lett. **101**, 130401 (2008); G. Theocharis, A. Weller, J. P. Ronzheimer, C. Gross, M. K. Oberthaler, P. G. Kevrekidis, and D. J. Frantzeskakis, "Multiple atomic dark solitons in cigar-shaped Bose-Einstein condensates," Phys. Rev. A **81**, 063604 (2010).

[53] W. H. Zurek, "Causality in condensates: gray solitons as relics of BEC formation," Phys. Rev. Lett. **102**, 105702 (2009).

[54] B. Damski and W. H. Zurek, "Soliton creation during a Bose-Einstein condensation," Phys. Rev. Lett. **104**, 160404 (2010).

[55] C. Lee, E. A. Ostrovskaya, and Y. S. Kivshar, "Nonlinearity-assisted quantum tunnelling in a matter-wave interferometer," J. Phys. B: At. Mol. Opt. Phys. **40**, 4235 (2007).

[56] Y. S. Kivshar, T. J. Alesander, and S. K. Turitsyn, "Nonlinear modes of a macroscopic quantum oscillator," Phys. Lett. A **278**, 225 (2001); S. Burger, L. D. Carr, P. Ohberg, K. Sengstock, and A. Sanpera, "Generation and interaction of solitons in Bose-Einstein condensates," Phys. Rev. A **65**, 043611 (2002).